



# Comprehensive Darcy-Scale Analysis of Ripening in Porous Media

Yitian Feng<sup>1,2</sup> · Chuanxi Wang<sup>1</sup> · Xu Jin<sup>3</sup> · Ke Xu<sup>1</sup> 

Received: 13 November 2021 / Accepted: 22 April 2022  
© The Author(s), under exclusive licence to Springer Nature B.V. 2022

## Abstract

Capillary trapping is considered as one of the safest geologic CO<sub>2</sub> storage mechanisms due to its hydrodynamic stability. However, the thermodynamic stability of capillary trapping was questioned by our recent work (Xu in *Geophys Res Lett* **46**(23):13804–13813, 2019). Gravity induces the top bubbles to grow at expense of bottom bubbles through the diffusion of dissolved gas components, that finally may form a gas cap and posing a risk of leakage, even in absence of convection. Here, we improve the gravity-induced ripening model introduced earlier and conduct theoretical and numerical analysis. Four regimes of bubble ripening are identified according to the modified Bond number and initial gas saturation, resulting in different scaling between the equilibrium time and the length scale. Vertical heterogeneity is also shown to have a great impact on the ripening process. When the permeability gradient is downward, the capillary pressure gradient competes with the gravitational gradient and results in a complex gas redistribution behavior. Capillarity dominates in a short time, while gravitational potential determines the global saturation profile in long term. This work provides a new physical perspective in evaluating CO<sub>2</sub> sequestration security and has a potential application in other porous systems that gas generated and evolve under strong external fields.

**Keywords** Bubble ripening · CO<sub>2</sub> sequestration · Diffusion · Capillary trapping

## 1 Introduction and Motivation

Ripening is a classical phenomenon that mass redistributes among dispersed phase clusters to reduce total surface energy (Lifshitz and Slyozov 1961; Slezov et al. 1993). In open space without geometric confinements and external fields, ripening always results in destabilization and coarsening of clusters (Beenakker and Ross 1985; Epstein and

---

✉ Ke Xu  
kexu1989@pku.edu.cn

<sup>1</sup> College of Engineering, Department of Energy and Resources Engineering, Peking University, Beijing, China

<sup>2</sup> College of Civil Engineering and Architecture, Zhejiang University, Hangzhou, China

<sup>3</sup> The Research Institute of Petroleum Exploration and Development, China National Petroleum Corporation, Beijing, China

Plesset 1950; Voorhees 1985; Wagner 1961). The reason is that smaller cluster always has larger surface curvature (thus larger capillary pressure,  $P_c$ ) and larger specific surface area (thus larger surface energy per mass), so driving mass from smaller clusters to larger clusters brings benefits of free energy reduction (Lifshitz and Slyozov 1961; Voorhees 1985). Ripening is therefore crucial in determining the stability and evolution of crystals, emulsion, bubble population, and foam (Mantzaris 2005; Meinders and van Vliet 2004; Venzl 1985; Yec and Zeng 2014).

In porous media, however, ripening becomes significantly different from that in open space. Bubbles' morphology, thus capillary pressure and surface energy, are regulated by the pore-throat confinement, which prevents bubbles from unlimited coarsening. Some recent work (de Chalendar et al. 2017; Wang et al. 2021; Xu et al. 2017) have shown the physics of bubble population ripening at pore scale by micromodel experiments and pore-network modeling—after ripening, bubbles evolve into a metastable distribution that all free surfaces share identical curvature (thus identical  $P_c$ ), and bubbles in porous media stop coarsening.

The pore-scale picture of bubble ripening further drives exploration of its Darcy scale effect. Li et al. (2020) set a Darcy-scale bubble ripening model and tested it in heterogeneous porous media, showing the trend of bubbles to evolve for low specific area regions. Further, our earlier work (Xu et al. 2019) proposed a simplified model which incorporates gravitational field. Gravity is shown to also be involved in the ripening process, inducing the dissolution of bubbles at the bottom to feed the growth of the bubble at the top. Gravity-induced ripening may again destabilize the capillary trapping of bubbles and lead to the formation of a gas cap. The vertical one-dimensional (1-D) continuum Darcy-scale equation depicting the gravity-induced ripening is constructed as:

$$\frac{\partial S}{\partial t} = \frac{\partial}{\partial z} \left( K \frac{\partial P_b}{\partial z} \right) \quad (1)$$

where  $P_b = P_c - \Delta\rho gz + P_0$  is the total potential of a bubble that considers both capillary pressure and gravitational potential.  $P_c$  is the local capillary pressure and  $P_0$  is the reference wetting phase pressure at  $z=0$ .  $P_0$  is assumed to be much larger than  $P_c$  (Bauget and Lenormand 2010).  $\Delta\rho$  is the density difference between liquid and gas.  $S$  is the gas saturation in stratum and  $K$  is the comprehensive rate constant. We show that the equation proposed by Li et al. (2020) is equivalent to Eq. (1) under certain assumptions in the supplemental material.

Although Eq. (1) has been proposed to discuss long-term possible destabilization of capillary trapping, quantitative analysis has not been provided yet about how competition between capillarity and gravity shapes the ripening kinetics. However, systematic and quantitative analysis is needed to determine the time scale of ripening compared with that of other CO<sub>2</sub> sequestration mechanisms, and to provide instant spatial phase distribution to further quantify geochemical reactions. In addition,  $K$  is assumed as a constant (which is exact only when every pore is occupied by a bubble) in the earlier work (Xu et al. 2019). Constant  $K$  results in fast diffusion at zero-saturation region, which fades the fact that the emergence of bubbles accelerates the mass transfer by shortening the diffusion distance in liquid phase from through the entire porous space to through only throats, and may results in numerical instability at the saturation front with sharp saturation jump.

Since a solid understanding of the ripening in porous media is of critical importance to evaluate the effectivity and efficiency of the capillarity trapping in the stratum,

comprehensive analysis of Darcy-scale ripening with gravity involved is required. Here we verify and modify Eq. (1). Analytical solutions are explored to predict the equilibrium time. We also establish a numerical simulation framework. The competition between gravity and capillarity at different spatial and temporal scales is investigated, by both analytical solutions and by numerical investigation of heterogeneity effects.

## 2 Model setup and Validation

### 2.1 Equations for Bubbles' State

$P_c$  in Eq. (1) is mainly determined by gas saturation  $S$ , pore geometry (size and shape), and wettability. To depict the relationship between capillarity pressure  $P_c$ , pore occupation  $C$  (defined as the portion of pores occupied by bubbles) and  $S$ , then simplify the model, we use the following  $P_c$ - $S$  and  $C$ - $S$  curves which is based on the models proposed in (Xu et al. 2019):

$$P_c = \begin{cases} \frac{P_{c,max} - P_{c,min}}{S_{max} - S_{crit}} (S - S_{crit}) + P_{c,min} & S_{crit} \leq S < S_{max} \\ P_{c,min} & \delta \leq S < S_{crit} \\ \frac{P_{c,min}}{\delta} S & S \leq \delta \end{cases} \quad (2)$$

$$C = \begin{cases} 1 & S \geq S_{crit} \\ \frac{S}{S_{crit}} & S < S_{crit} \end{cases} \quad (3)$$

This set of equations is established based on a conceptual physical model for homogeneous porous media with uniform pore size.  $S_{crit}$  is a critical saturation, when  $S = S_{crit}$ , all pores are occupied by bubbles at the critical volume, i.e., of the shape of the largest possible sphere in a pore-body that is tangent to the solid wall of the pore. At this status, the bubble's capillary pressure is at its minimum possible value in the porous media,  $P_{c,min}$ .

When  $0 < S < S_{crit}$ , not all pores may be occupied by bubbles at a metastable condition; elsewhere, at least some bubbles are free spheres and classical ripening emerges so that some bubbles dissolve to feed others until all remaining bubbles reach  $P_c = P_{c,min}$ . The pore occupancy,  $C$ , can be calculated by assuming all remaining bubbles are at the critical volume. When  $S > S_{crit}$ , bubbles are deformed by pore geometry and  $P_c$  increases with  $S$ , in which regime  $C = 1$ . The saturation at which bubbles penetrate the throats and connect to be continuous gas phase is set as  $S_{max}$ , corresponding to a maximum capillary pressure  $P_{c,max}$ . In addition,  $P_c = 0$  when  $S = 0$ , so we set a linear "jump" of  $P_c$  from 0 to  $P_{c,min}$  when  $S$  increases from 0 to  $\delta$ , where  $\delta < 1$ . This "jump" reflects the physical limit that infinitely small curvature cannot exist for a non-wetting phase in porous media—a minimum  $P_c$  does exist, corresponding to the largest sphere in a pore body that is tangent to the solid wall of the pore. The jump at  $[0, \delta]$  is another major improvement compared to our earlier model, which not only better demonstrate the continuity of capillary pressure at low saturation extreme, but also eliminates numerical instability at near-zero saturation region. We note that  $P_c$  for bubble population is physically distinct from the  $P_c$  for the continuous gas phase in fluid–fluid displacement, as bubbles are hydrodynamically disconnected and interacting through diffusion, while a continuous gas phase is internally hydrodynamically connected.  $S_{crit}$ ,  $S_{max}$  and  $P_{c,max}/P_{c,min}$  only depends on pore shape rather than the pore

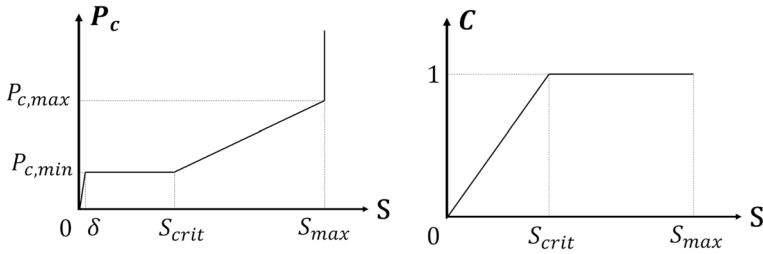


**Fig. 1** And for a capillary trapped bubble population (Xu et al. 2019)

size. We denote  $\Delta P_C = P_{C,max} - P_{C,min}$ ,  $\Delta S = S_{max} - S_{crit}$ , and  $P = \Delta P_C / \Delta S$ . We plot the function of  $P_C(S)$  and  $C(S)$  in Fig. 1 for a better understanding.

## 2.2 Mass Transfer Coefficient

The mass conservation equation for ripening is in form of Eq. (1). The flux of saturation is thus written as

$$J = -K \frac{\partial P_b}{\partial z} \quad (4)$$

In our earlier work,  $K$  is assumed to be a constant determined by pore structure. However, we show that it should be also a function of bubble saturation: in a pore that is not occupied by bubble, gas needs to diffuse through both pore body and pore-throat in the liquid phase; while in a pore that is occupied by a bubble, the diffusion through pore-body is in the gas phase, which is infinitely faster than that in the liquid phase. Therefore, a gas-occupied pore should have a much faster gas diffusion coefficient than a liquid-saturated pore, thus  $K$  should be a function of  $C$ . When  $C=1$  (all pores are occupied by bubbles), gas transfers through pore throats only. We denote the mass transfer rate constant at  $C=1$  as  $K^*$ . When  $C=0$  (bubble-free zone), gas has to transfer through not only the pore throats but also the pore bodies by internal convection. In this situation, mass transfer rate  $K=K_0$  may be 1–2 orders of magnitude smaller than  $K^*$  because of enlarged transfer distance and tortuosity, details are shown in the supplemental material. We then formulate the general form of  $K$  for arbitrary  $C$ , as:

$$K = K^* C + K_0(1 - C) \quad (5)$$

For simplicity, we make some assumptions. We assume that the thickness of the strata,  $H$ , is much small than the depth of the stratum, so  $|P_C - \Delta \rho g H| \ll P_0$ . The density variation for both phases can therefore be assumed as constant. The temperature gradient can also be neglected. We neglect the change of mass in the gas phase, as the mass variation of dissolve gas for different gas-phase distribution can be neglected compared to gas-phase mass. Convection is ignored and mass transfer in the system only results from ripening. Validation of these assumptions is discussed in the supplemental material.

We note that  $K$  is of similar dimension to mobility in Darcy's law. In typical  $\text{CO}_2$  sequestration scenario, the value of  $K^*$  is about  $\sim 10^{-16} \text{ m}^2/\text{Pa}\cdot\text{s}$ , that corresponds to permeability of  $\sim 10^{-20} \text{ m}^2$  ( $\sim 10^1 \text{ nD}$ ). Nevertheless, as the gas are in capillary trapping

status, its actual hydrodynamic mobility is exactly zero. Therefore, although the ripening appears equivalent to hydrodynamic flow at very low permeability, it is not overwhelmed by viscous flow due to gas’s bubble state.

### 2.3 Dimensionless Form

We rewrite Eq. (1) in dimensionless form as:

$$\frac{\partial S}{\partial \tilde{t}} = \frac{\partial}{\partial \tilde{z}} \left[ \tilde{K} \cdot \frac{\partial}{\partial \tilde{z}} \left( \tilde{P}_C - Bo^* \tilde{z} \right) \right] \tag{6}$$

where  $\tilde{z} = z/H$  is the dimensionless height,  $\tilde{P}_C = P_c/\Delta P_c$  is the dimensionless capillary pressure,  $\tilde{t} = PK^*t/H^2$  is the dimensionless time, and  $\tilde{K} = K/K^*$  is the dimensionless rate coefficient.  $Bo^* = \Delta\rho gH / \Delta P_c$  is modified Bond Number. When  $Bo^* \gg 1$ , gravity is the dominant driving force and capillary force is only locally important. When  $Bo^* \ll 1$ , capillarity effect is the global dominant driving force and gravity can be neglected. Completely neglecting gravity yields  $Bo^* = 0$ .

To compare the ripening time in different conditions, we define a dimensionless characteristic time:  $t_c = H^2/K^*P(1 + Bo^*)$ . If  $Bo^* \ll 1$ ,  $t_c$  could be simplified as  $H^2/K^*P$ . If  $Bo^* \gg 1$ ,  $t_c$  could be simplified as  $H^2/K^*Bo^*P$ .

## 3 Ripening in Homogeneous Media

In this section, we analyze the ripening of bubbles in homogenous porous medium. Here “homogeneous” implies that the  $P_c$ - $S$  function,  $C$ - $S$  function, and  $K$ - $S$  function are all identical in the entire domain. For convenience, we only consider strata that are confined by impermeable upper and bottom boundaries in this section for simple analysis, so  $J=0$  at  $z=0$  and at  $z=H$ . The boundary condition could be modified in practical calculations.

### 3.1 Scaling and Analytical Solutions

Gravity effect plays significant role in ripening process that dissolves deeper bubbles, drives dissolved gas to diffuse upward, and then grows bubbles at the top. At equilibrium, a bubble-free zone is left at the bottom, and a continuous gas cap under the caprock is formed. It should be noted that the “bubble-free zone” in this work is not free of the bubble. A very small amount of gas ( $S \leq \delta$ ) still may exist in this region. At equilibrium,  $\partial S/\partial \tilde{t} = 0$ . By cancelling the time-dependent term in Eq. (6), we can get:

$$\frac{dS}{d\tilde{z}} = Bo^* \Delta S \tag{7}$$

It means that a stable capillary trapping belt (SCTB) exists between the gas cap and the bubble-free zone at equilibrium, and the dimensionless slope of SCTB is  $Bo^* \Delta S$ . In SCTB, gas is still in bubble form and can be hydrodynamically immobile.  $Bo^*$  is thus the most significant indicator of the dominant driving force. If  $Bo^* \gg 1$ , the SCTB would be extremely short and we only expect the final emergence of gas cap and gas-free zone; in contrast, if  $Bo^* \ll 1$ , the calculated SCTB can be even larger than the whole domain, so all bubbles may be stably trapped.

In addition, we note that whether the mean residual saturation  $S_r$  exceeds  $S_{crit}$  is another important parameter that determines the ripening kinetics, which is not unique to our ideal model of  $P_C(S)$  and  $C(S)$  in Eqs. (2) and (3): a slowly changed  $P_C$  at low  $S$  and a fast-increasing  $P_C$  at high  $S$  is general for most cases (Bear 1996; 2013; Lake et al. 2014).

Accordingly, we could identify 4 regimes of bubble ripening in the  $Bo^*-S_r$  space:

- Regime I:  $Bo^* \gg 1, S_r > S_{crit}$ ;
- Regime II:  $Bo^* \gg 1, S_r < S_{crit}$ ;
- Regime III:  $Bo^* \ll 1, S_r > S_{crit}$ ;
- Regime IV:  $Bo^* \ll 1, S_r < S_{crit}$ .

In this section, we set up scaling arguments between equilibrium time  $t_{eq}$  and the space scale in each regime.

### 3.1.1 Analysis of Regime III

In Regime III,  $Bo^* \ll 1$  and capillarity plays a dominant role when  $S \in [S_{crit}, S_{crit}]$ . Accordingly,  $Bo^*$  is small and could be neglected compared to the capillary potential gradient. In addition,  $C = 1$  always holds so  $\tilde{K} = 1$ . Equation (6) could then be rewritten as:

$$\frac{\partial S}{\partial t} \approx \frac{\partial}{\partial \tilde{z}} \left( \frac{\partial \tilde{P}_C}{\partial \tilde{z}} \right) \tag{8}$$

It is in form of simple diffusion equation. Taking into consideration that linear correlation is set between  $\tilde{P}_C$  and  $S$  when  $S \in [S_{crit}, S_{crit}]$ , dimensional analysis of Eq. (8) yields the scaling between time  $\Delta t$  and the corresponding change in stratum thickness  $\Delta h$ :

$$\frac{1}{\Delta t} \sim \frac{1}{\Delta h^2} \tag{9}$$

Therefore, we could estimate that  $t_{eq} \sim H^2$  in Regime III. This scaling can be verified by an analytic solution. With the Eq. (6) and boundary condition  $J(z=0, z=H) = 0$ , we could compute the ripening process. For simplicity, we only keep the first term of the Fourier expansion of the solution, which could be described as:

$$S \approx S_r + \Delta S \cdot Bo^* \left( \tilde{z} - \frac{1}{2} \right) + \frac{4\Delta S \cdot Bo^*}{\pi^2} \cos \pi \tilde{z} \cdot e^{-\frac{K^* P \pi^2 t}{H^2}} \tag{10}$$

The first two terms in this analytical solution correspond to the equilibrium profile. The amplitude of the last term decreases sharply with time, and this term transfers the profile from fluctuant to linear. We note that when  $K^* P t / H^2 = 0.4$ , the last term is small enough and the system is nearly equilibrated. Then, we define the equilibrium time  $t_{eq} = 0.4 H^2 / K^* P \sim 0.4 t_c$ . Easy to see that  $t_{eq} \sim H^2$ , just as the classical diffusion (Deen 1998).

At the equilibrium, gravity only minorly modifies the saturation profile, and the whole domain is in SCTB. The whole stratum is thus stably trapping the bubbles. If gravity is totally ignored ( $Bo^* = 0$ ), the slope of SCTB is zero, saturation will tend to be uniform and equilibrate at  $S_r$ .

### 3.1.2 Analysis of Regime I, II, and IV

In Regime I and Regime II,  $Bo^* \gg 1$ , thus gravity dominates. According to Eq. (7), the slope of SCTB is sharp and the capillary trapping region is negligible compared to the domain size. Dissolved gas will transfer upward and gathers as a gas cap at the top. The diffusion flux could be simplified as  $J \approx -K\Delta\rho g$  as we neglect the capillary effect.

In Regime IV,  $Bo^* \gg 1$  and the initial saturation  $S_r < S_{crit}$ . According to Eq. (2),  $P_C = P_{C, min}$  is a constant, so the diffusion flux  $J = K\Delta\rho g$ . Therefore, gas still moves upward driven by gravitational potential regardless of small  $Bo^*$ . When the saturation increases to  $S_{crit}$ , capillary pressure becomes very sensitive to  $S$ , and even small increase of  $S$  would induce huge pressure gradient. Therefore, according to Eq. (6), the saturation gradient in  $S > S_{crit}$  region can be neglected, appearing like a plateau of saturation near  $S_{crit}$ .

Therefore, the redistribution kinetics in these three regimes could be reduced to one form: gas is vertically transferred with diffusion flux  $J = K\Delta\rho g$  toward a plateau of fixed  $S$  where diffusion flux  $J$  reduces to 0. We could thus simplify the saturation profile during the evolution to be a constant function.

$$S = \begin{cases} S_{eq} z \geq z_t \\ S_r z_b \leq z < z_t \\ 0 z < z_b \end{cases} \tag{11}$$

where  $S_{eq} = S_{max}$  for Regime I and II,  $S_{eq} = S_{crit}$  for Regime IV,  $z_t$  and  $z_b$  are the top front and the bottom front of the initial saturation zone. According to Eq. (6), the relation between time  $\Delta t$  and the corresponding change in  $\Delta z_t$  and  $\Delta z_b$  could be written as:

$$\frac{S_{eq} - S_r}{\Delta t} \approx \frac{0 - (-K\Delta\rho g)}{\Delta z_t} \tag{12}$$

$$\frac{S_r - 0}{\Delta t} \approx \frac{0 - (-K\Delta\rho g)}{\Delta z_b} \tag{13}$$

We could therefore identify the scaling of  $t_{eq} \sim H$  in this situation. We get the analytical solution of equilibrium time, which verifies the scaling relation is in a simple form:

$$t_{eq} = \frac{H}{K\Delta\rho g} \cdot \frac{S_r(S_{eq} - S_r)}{S_{eq}} \tag{14}$$

Detailed deduction could be seen in the *Supplemental Information*.

These above analytical solutions would help us to estimate the actual time scale of ripening process. We use a 2 m thin strata at 2 km deep and with CO<sub>2</sub>-water system as an example. If  $S = 0.4$  and  $Bo^* \gg 1$ , the gas cap may form in top 50% space of this strata, according to Eq. (12), that is shorter than effective mineral trapping time scale, and the equilibrium time is 8000 years. Nevertheless, for a 20 m strata, the equilibrium time is 80000 years, that is comparable with mineral trapping; nevertheless, the ripening spatially redistributes the fluid, so the fluid-reaction relation is still affected by this ripening process.

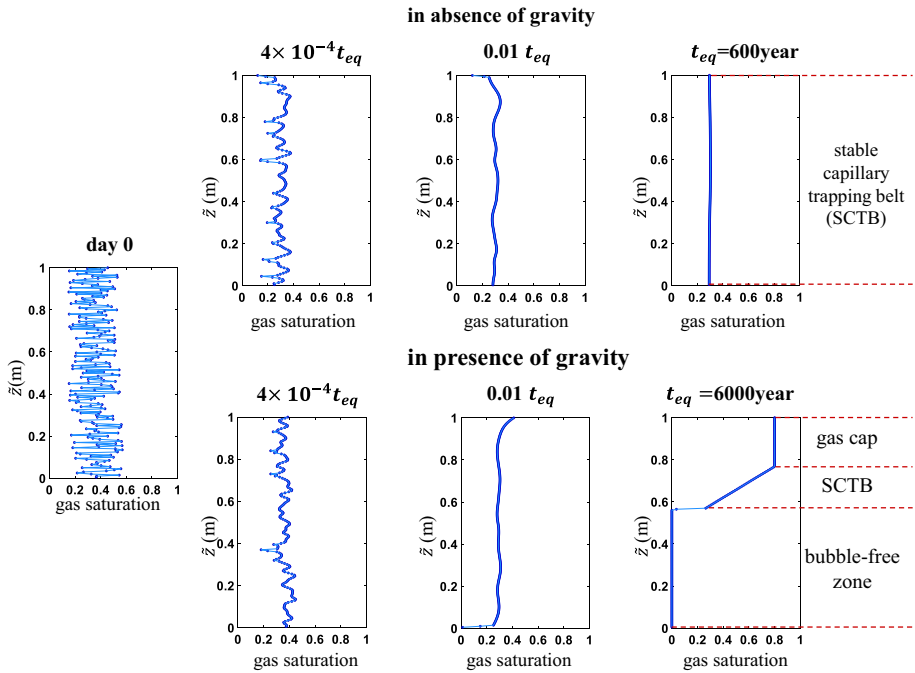


**Fig. 2** Evolution of saturation profile in a 1 m thick strata. We set  $P_{C, max}=2333$  Pa,  $P_{C, min}=800$  Pa,  $H=1$  m. We denote  $t_{eq}$  as the time for equilibrium. In this paper, when the total error  $\int_0^1 |S - S_{t \rightarrow \infty}| dz < 1 \times 10^{-4}$ , we think equilibrium is already achieved

### 3.2 Numerical Simulation for Homogeneous Media

Numerical simulation in 1-D can be conducted using finite differential method. Detailed discussion and numerical process of this part could be seen in the *Supplemental Information*. Without loss of generality, we set  $S_{crit}=0.3$ ,  $S_{max}=0.8$  in the following case studies. Gas and liquid properties correspond to 10 MPa and 60 °C CO<sub>2</sub> and water, which is among reasonable CO<sub>2</sub> sequestration operation range. We set  $K^*=2.81 \times 10^{-16}$  m<sup>2</sup>/P<sub>a</sub>.s,  $K_0=4.01 \times 10^{-18}$  m<sup>2</sup>/P<sub>a</sub>.s. Details are shown in the supplemental material.

#### 3.2.1 Qualitative Demonstration of Gravity Effect

Figure 2 shows the comparison between no-gravity ripening and gravity-assisted ripening. The new model well reproduced our earlier results using old model, in this ideal scenario. It shows that in the absence of flow, gravity induces the growth of bubbles at the top at expense of dissolution of bubbles at the bottom. The time scale for local capillary equilibrium is within hundreds of years that is much shorter than mineral trapping; however, the time scale for equilibrium is ~6000 years that is mildly shorter than mineral trapping. The formation of gas cap may pose the risk of leakage.

### 3.2.2 Ripening Kinetics in Four Regimes

We conduct numerical simulations for four regimes. Key parameters are:

- Regime I:  $H=23$  m,  $P_{C, \max}=2333$  Pa,  $P_{C, \min}=800$  Pa,  $Bo^*=98$ ,  $S_r=0.2$ ,  $t_c=2 \times 10^5$  year
- Regime II:  $H=23$  m,  $P_{C, \max}=2333$  Pa,  $P_{C, \min}=800$  Pa,  $Bo^*=98$ ,  $S_r=0.5$ ,  $t_c=2 \times 10^5$  year;
- Regime III:  $H=0.1$  m,  $P_{C, \max}=23333$  Pa,  $P_{C, \min}=8000$  Pa,  $Bo^*=0.05$ ,  $S_r=0.2$ ,  $t_c=35$  year;
- Regime IV:  $H=0.1$  m,  $P_{C, \max}=23333$  Pa,  $P_{C, \min}=8000$  Pa,  $Bo^*=0.05$ ,  $S_r=$ ,  $t_c=35$  year;

We compare the analytical solutions for all four regimes against numerical simulation results, as shown in Fig. 3. It shows that the kinetics and saturation profile in simulation are in good matching with analytical solutions.

In addition, numerical simulations validate the scaling argument we derived earlier. If  $S_r > S_{crit}$  the equilibrium time  $t_{eq}$  is proportional to  $H^2$  when  $Bo^* \ll 1$ , and proportional to  $H$  when  $Bo^* \gg 1$ ; If  $S_r < S_{crit}$ ,  $t_{eq}$  is proportional to  $H$  regardless of  $S_r$ , although the pre-factor is different for  $Bo^* \ll 1$  and  $Bo^* \gg 1$ . If the stratum has a small thickness and small pores ( $Bo^* \ll 1$ ), gas saturation is moderate ( $S_r > S_{crit}$ ), capillary trapping will have the biggest efficiency.

## 4 Ripening in Strata with Spatial Contrast of Pore Size

Real strata are heterogeneous that the average pore size varies significantly, especially in the vertical dimension, as they consist of a sequence of different thin layers. Although the diffusion coefficient's change with porosity and tortuosity are always relatively minor (Saripalli et al. 2002), the pore size change may results in  $P_c$  change over several orders of magnitudes that poses additional driving force to ripening. Therefore, it is necessary to study the influence of pore size heterogeneity on the diffusive evolution.

In this section, we focus on a simplified case that the domain consists of two regions with pore size contrast. Two domains are of same thickness.  $H_1=H_2=H/2$ . We donate the upper one as domain 1 and the lower one as domain 2. The two domains are different in pore sizes, so the function  $P_c$ - $S$  are different for the two domains. All other properties such as pore shape are the same, so the value of  $K$ ,  $S_{crit}$ , and  $S_{max}$  in two domains are identical.

To quantify the  $P_c$  contrast, we define  $\gamma = \Delta P_{C, 2} / \Delta P_{C, 1}$ . When conducting numerical simulations, we set  $S_{crit}=0.3$ ,  $S_{max}=0.8$ , the initial saturation  $S_r$  and other properties are the same in two domains.

### 4.1 Redistribution in Absence of Gravity

We first consider the no-gravity case. Ripening is driven only by the  $P_c$  contrast between the two domains that depends on  $\gamma$ . Without loss of generality, we set domain 2 is of larger  $P_c$  so  $\gamma > 1$ . Gas transfers from domain 1 to domain 2 until the two domains share the same capillary pressure.

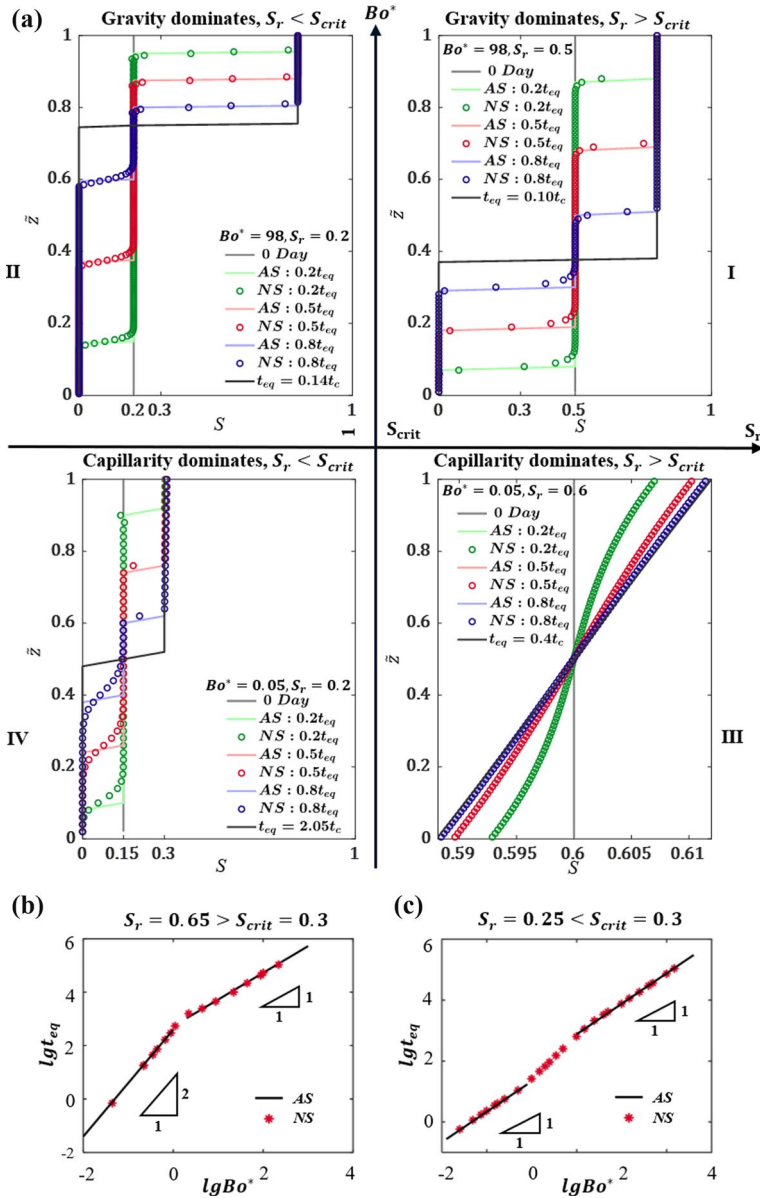


**Fig. 3** The up row: **a** comparison between numerical simulation(NS) and analytical solutions(AS) of 4 types of the ripening process in homogeneous strata. In regime I,  $S_r > S_{crit}$ ,  $Bo^* > > 1$ , the thick gas cap will form with a high risk of leakage. In regime II,  $S_r < S_{crit}$ ,  $Bo^* > > 1$ , the thickness of the gas cap is smaller than regime I because of the small gas amount. In regime III,  $S_r > S_{crit}$ ,  $Bo^* < < 1$ , the whole strata could trap bubbles stably. It's the most efficient trapping condition. In regime IV,  $S_r < S_{crit}$ ,  $Bo^* < < 1$ , SCTB is small because of the small gas amount. In conclusion, if  $Bo^* < < 1$ , increasing the concentration of the injected gas can improve the efficiency of storage; but if  $Bo^* > > 1$ , the efficiency of storage cannot be increased by  $S_r$ , and the safety of trapping is reduced because of the existence of a thick gas cap. The low row: Scaling relation between  $t_{eq}$  and  $H$ . **b**  $S_r < S_{crit}$ ,  $t_{eq} \sim H$  regardless of  $Bo^*$  with a different coefficient. **c**  $S_r > S_{crit}$ ,  $t_{eq} \sim H$  when  $Bo^* > 1$  and when  $t_{eq} \sim H^2$  when  $Bo^* < 1$

If  $\gamma$  approximates to 1, the heterogeneity is weak, and the equilibrium could be approached with slight saturation redistribution. It qualitatively matches Li et al. (2022). An analytical solution can be derived as:

$$P_{c1}(z, t) = \sum_{m=1}^{\infty} B_m \cos\left(2\mu\lambda_m \frac{H-z}{H}\right) e^{-\beta_m t} \tag{15a}$$

$$P_{c2}(z, t) = \sum_{m=1}^{\infty} A_m B_m \cos\left(\lambda_m \frac{2z}{H}\right) e^{-\beta_m t} \tag{15b}$$

where  $\mu = \sqrt{\gamma}$ ,  $\tan(\lambda_m) = -\mu \tan(\mu\lambda_m)$ ,  $\beta_m = -\frac{KP_2\lambda_m^2}{H^2/4}$ ,  $A_m = \frac{\cos(\mu\lambda_m)}{\cos(\lambda_m)}$ ,  $B_m = \frac{2\sin(\lambda_m)A_m(P_{c2,0} - P_{c1,0})}{\lambda_m(A_m^2 + \gamma)}$ ,  $P_{c1,0}$ ,  $P_{c2,0}$  are the initial capillary pressure in the two domains, respectively. The detailed deduction could be seen in the supplemental material.

However, when  $\gamma \gg 1$ , even  $P_{c, min}$  in domain 2 is larger than  $P_{C,max}$  in domain 1. As a result, the mass in domain 2 has to merge into domain 1, until saturation in domain 2 drops below  $\delta$  or saturation in domain 1 grows to  $S_{max}$ . Under this condition, gas saturation in domain 2 will first decrease to  $S_{crit}$  soon enough, and the diffusion flux at the boundary decreases sharply because of the smaller rate constant  $K_0$  once bubble-free zone forms. Then the bubble-free zone enlarges, and diffusion flux continues to decrease because of the transfer distance enlargement. We note that this case highlights the necessity

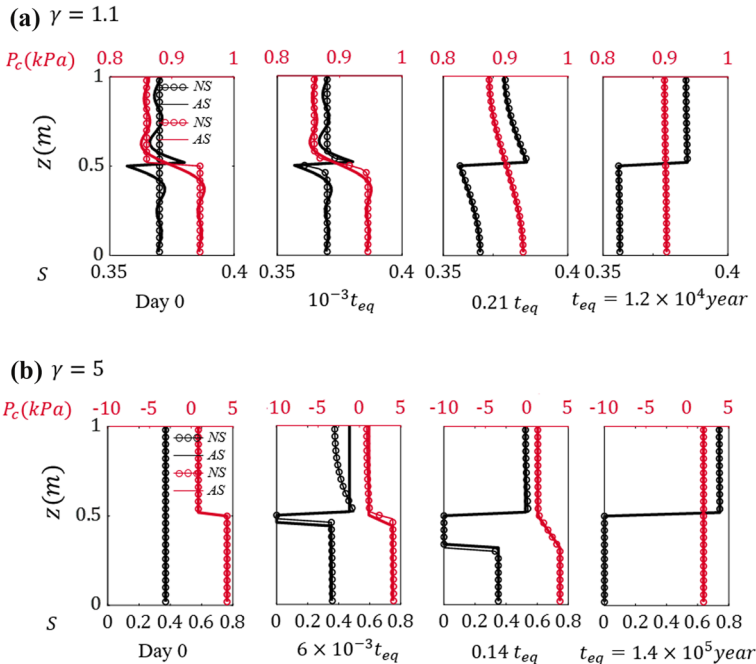


**Fig. 4** Comparison between numerical simulation (NS) and analytical solutions (AS) of evolution process in heterogeneous strata. **a**  $\gamma = 1.1$ , capillarity contrast is small. Capillarity drives bubbles in domain 2 with higher  $P_C$  to domain 1 with smaller  $P_C$ . At equilibrium, the saturation profile is slightly redistributed in a small range. **b**  $\gamma = 5$ , capillarity contrast is huge. The bubble-free zone will form in domain 2 until all bubbles in domain 2 transfer to domain 1. When the bubble free zone appears, the ripening process slows down

of modification in  $K$  (Eq. 5), without which the kinetics would be highly overestimated. We denote  $h_b$  as the thickness of the bubble-free zone. we get the analytical solution to figure out the relationship between  $t$  and  $h_b$ :

$$t = \frac{S_r}{K_0 A^2} \left( -A h_b - B \ln \left( 1 - \frac{A}{B} h_b \right) \right) \tag{16}$$

where  $A = \frac{2P_1 S_r}{H}$ ,  $B = \Delta P_{c1} \left( \frac{\gamma-1}{F-1} - 2 \frac{S_r - S_{crit}}{\Delta S} \right)$ . This solution validates that the rate of the ripening process decreases as the bubble-free zone enlarges.

The numerical solutions of ripening kinetics for both  $\gamma \sim 1$  and  $\gamma > 1$  cases are shown in Fig. 4. Both the evolution of  $S$  (black lines) and the evolution of  $P_c$  (red lines) are shown. We thus clearly demonstrate the separation of saturation with homogenization of

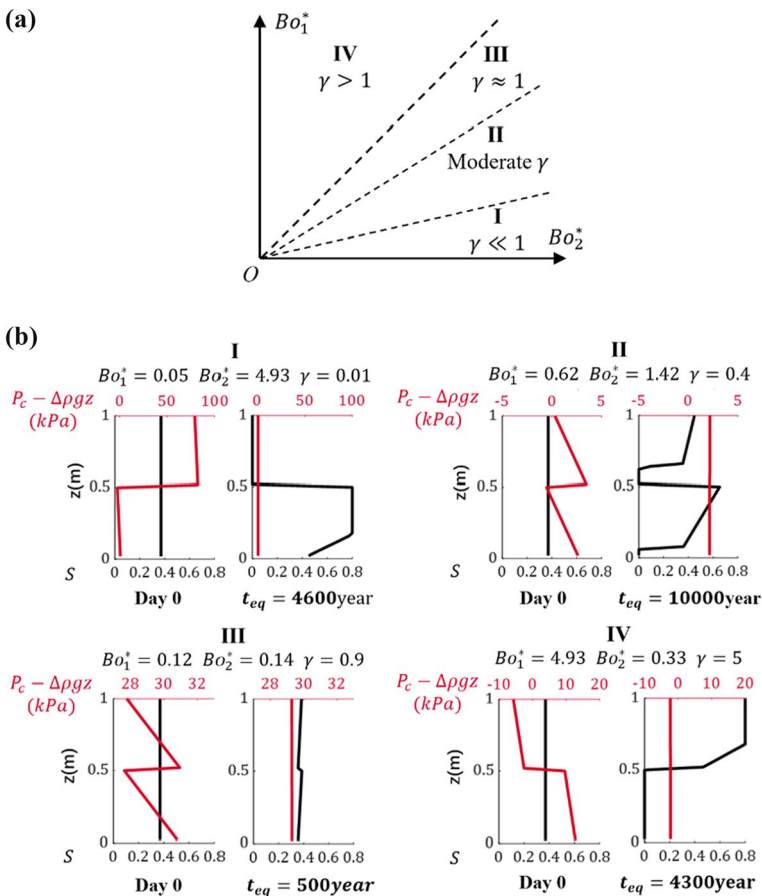


**Fig. 5** **a** Quadrant division for bubble ripening in heterogeneous strata in the presence of gravity. **b** Numerical simulations for bubble evolution in 4 Regime.  $\gamma > 1$ , the bottom stratum has the bigger  $P_c$ , heterogeneity strengthens the upward transfer.  $\gamma < 1$ , the top stratum has the bigger  $P_c$ . If only considering capillarity, gas will transfer downward contrary to the gravitational trend. At equilibrium, gas is multi-layer distributed when  $\gamma$  is moderate

capillary pressure. We note that ripening without gravity in heterogeneous strata may take a long time.

### 4.2 Redistribution with Both Gravity and Capillarity Contrast

Gravitational gradient drives the bubbles upward and is invariable all the time, while capillary gradient drives the gas to migrate along pore size gradient. Therefore, we identify 4 regimes of bubble ripening by  $\gamma$ ,  $Bo^*_1$  and  $Bo^*_2$  shown as Fig. 5a. Regime I:  $\gamma < 1$ , Regime II:  $\gamma < 1$ , moderate  $\gamma$ , Regime III:  $\gamma < 1, \gamma \approx 1$ , Regime IV:  $\gamma > 1$ .

For Regime IV,  $\gamma > 1$ . It indicates that the lower stratum has the bigger capillary pressure. Gravitational gradient and capillary pressure are thus synergistically driving the gas upward. The competition between gravity effect and capillary effect is much similar to the ripening in homogeneous strata, although with qualitatively different kinetics.

For Regime I to Regime III,  $\gamma < 1$ . In such cases, capillarity drives gas downward, while gravity drives gas upward. In Regime III with negligible capillarity contrast, gas saturation will redistribute just as in the homogeneous stratum. In Regime I with huge capillarity contrast, all the bubbles transfer to the lower stratum, and the effect of gravity could be ignored. However, with moderate  $\gamma$ , as in Regime II, a big capillary pressure difference drives gas transfer toward domain 2 (the lower one) and generates a bubble-free zone between them. We denote the pressure at the two boundaries of the bubble-free zone as  $P_{b, upper}$  (small invariable gravitational pressure and bigger variable capillary pressure) and  $P_{b, lower}$ . As  $P_{b, upper} = P_{b, lower}$  the system is balanced overall. Therefore, continuous strata may be separated into two layers by a bubble-free zone as a result of the conflicting capillary potential contrast and gravity potential gradient. In Supplemental Material, we make a simple estimation about the scope of  $\gamma$  for Regime II.

The numerical solutions of ripening kinetics for both  $\gamma \sim 1$  and  $\gamma > 1$  cases are shown in Fig. 5. Both the evolution of S (black lines) and the evolution of  $P_C - \Delta\rho gz$  (red lines) are shown. We thus clearly demonstrate the separation of saturation with homogenization of total potential. In presence of gravity, equilibrium time of ripening in heterogeneous strata may shorter than  $10^4$ , gas cap may form before mineral trapping taking effect.

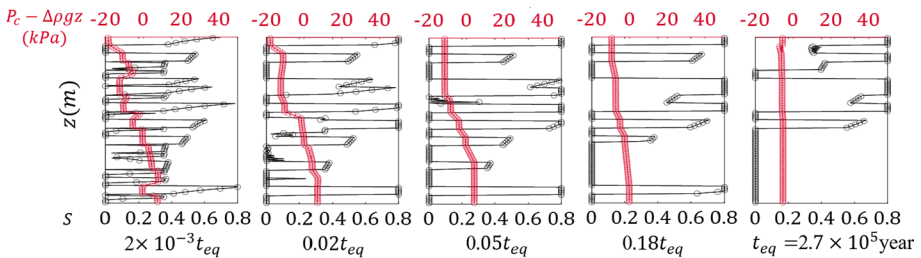


**Fig. 6** The numerical simulation for bubble evolution in 20-layer heterogeneous strata. In the beginning, gas will be separated into multiple domains. And for the long term, gas tends to move upward but strata with huge  $P_C$  will still be free of gas

## 5 Ripening in Multi-Layer Heterogeneous Media

To be more practical, we set 20 layers in series with capillary pressure changing from  $\Delta P_C$  changes from  $2.31 \times 10^2$  Pa to  $1.01 \times 10^4$  Pa randomly. The total height of the strata is 10 m. The ripening process is shown in Fig. 6. In the beginning, capillarity dominates locally, and the total potential of bubbles in strata tends to be uniform. Gas will be separated by multiple layers because of the pore size contrast. Strata with smaller pores and bigger capillary pressure may form a bubble-free zone and strata with bigger pores and smaller capillary pressure may form a gas cap. Later, because the mean Bond number is much larger than 1, gravity is still the globally dominant driving force in the long-term time. It takes  $2.7 \times 10^5$  years for ripening equilibrium.

The results show that, capillarity dominates local distribution of gas that concentrates local saturation in domains with low  $P_c$ ; however, for the whole strata, gravitational gradient dominates, that moves gas upward globally. The scale of capillarity and gravity in ripening can thus be separated.

## 6 Limitations and Implications

We note that convection itself plays a crucial role in gas redistribution hydrodynamically (Nield and Bejan 2006). Due to the unfavored density distribution, circumflux may emerge that enhances the mass transfer (Ho et al. 1998). It should be studied in future investigation to better predict the kinetics. Nevertheless, we emphasize that, in a close system, such circumflux may not change the final thermodynamic stable profile.

In addition, we also neglect chemical reactions, which should be considered in a practical scenario. According to IPCC 2006 (Eggleston et al. 2006), chemical reactions result in mineral trapping, which becomes important after thousands of years. As this time scale may have some overlap with the ripening process, more practical study is needed further to estimate the interplay between chemical reactions and ripening.

Vertical variation of gas solubility, 3-D effects, and the geothermal gradient are not discussed here, which is acceptable only when the stratum thickness is much smaller than the depth. If we are to consider these factors, analytical solutions become non-trivial, and complicated numerical simulations are required. A detailed study is deferred to the future.

Unfortunately, due to its long time scale, experiments are currently not available to validate the gravity-induced ripening in porous media. Appropriate design may provide future experimental evidence or challenge to the theory. For example, the gravitational acceleration can be amplified by centrifuge; careful selection of high-solubility and low-tension system can help to reduce the time scale.

We also note that this ripening may not be the only important in  $\text{CO}_2$  sequestration. It may be even more significant in many small-scale scenarios, such as the relaxation process after intensive degassing process during oil and gas recovery (Lake et al. 2014; Lee et al. 2016), and water management in a fuel cell (Andersson et al. 2016; Lu et al. 2010). If strong external fields exist, such as extreme temperature gradient, such as that in porous heat exchanger for MEM systems (Kim et al. 2000), similar phenomena may also happen.

## 7 Conclusion

We modify the Darcy-scale model of Ostwald ripening in porous media to incorporate the influence of gas bubbles in mass transfer. By introducing a simplified  $P_c(S)$  function, we can derive analytical solutions for the evolution kinetics and equilibrium states of gas redistribution under extreme ideal conditions. Simple 1-D numerical simulation is also conducted.

It is found that gravitational potential can drive upward migration of  $\text{CO}_2$  even in absence of convection. The gas cap may finally form even all gas is initially trapped as bubbles when the Bond number is much larger than 1. Four regimes of bubble ripening are identified according to the Bond number and initial gas saturation, with analytical solution achieved. Through the analytical solution and numerical simulation, we calculate the proportional relationship with the equilibrium time  $t_{eq}$  and the space scale  $H$ . Only when  $Bo^* \ll 1$  and  $S_r > S_{crit}$ ,  $t_{eq} \sim H^2$  just as the classical diffusion. In other situations,  $t_{eq} \sim H$ . Analytical solutions match well with numerical simulation results.

What's more, we show that pore size heterogeneity has a great impact on the ripening process. When the pore size gradient is downward, the capillary pressure gradient is competing with the gravitational gradient and results in complex gas redistribution behavior. We derive analytical solutions for simple two-layer models. For a more complex multi-layer case, we show that capillarity dominates and shapes the local saturation profile in a short time, while gravitational potential still determines the global saturation profile in long term.

This approach may have a potential application, not only in estimating carbon sequestration safety but also in porous systems that gas generated and evolve under strong external fields.

**Supplementary Information** The online version contains supplementary material available at <https://doi.org/10.1007/s11242-022-01794-4>.

**Acknowledgements** We gratefully acknowledge the financial support and funding from National Natural Science Foundation of China under Grant No. 12172010, and from CNPC Research Institute of Petroleum Exploration and Development for the project "Key Fluid Mechanisms of  $\text{CO}_2$ -EOR for Gu-Long Shale Oil Development". We also benefited a lot from helpful discussions with Dr. Sally Benson at Stanford University during the conference AGU2019.

## References

- Andersson, M., Beale, S.B., Espinoza, M., Wu, Z., Lehnert, W.: A review of cell-scale multiphase flow modeling, including water management, in polymer electrolyte fuel cells. *Appl. Energy* **180**, 757–778 (2016)
- Bauget, F., Lenormand, R.: Mechanisms of bubble formation by pressure decline in porous media: a critical review. *SOCAR Proc.* 2010(3), (2010)
- Bear, J.: *Modeling Phenomena of Flow and Transport in Porous Media*. Springer International Publishing, Cham (1996)
- Bear, J.: *Dynamics of Fluids in Porous Media*. Courier Corporation, Massachusetts (2013)
- Beenakker, C.W.J., Ross, J.: Theory of Ostwald ripening for open systems. *J. Chem. Phys.* **83**(9), 4710–4714 (1985)
- de Chalendar, J.A., Garing, C., Benson, S.M.: Pore-scale modelling of Ostwald ripening. *J. Fluid Mech.* **835**, 363–392 (2017)
- Deen, W.M.: *Analysis of Transport Phenomena*. Oxford USA profession, Oxford (1998)

- Eggleston, H., Buendia, L., Miwa, K., Ngara, T., Tanabe, K.: 2006 IPCC guidelines for national greenhouse gas inventories. (2006)
- Epstein, P.S., Plesset, M.S.: On the stability of gas bubbles in liquid-gas solutions. *J. Chem. Phys.* **18**(11), 1505–1509 (1950)
- Ho, C.-D., Yeh, H.-M., Sheu, W.-S.: An analytical study of heat and mass transfer through a parallel-plate channel with recycle. *Int. J. Heat Mass Transf.* **41**(17), 2589–2599 (1998)
- Kim, S., Paek, J., Kang, B.: Flow and heat transfer correlations for porous fin in a plate-fin heat exchanger. *J. Heat Transfer* **122**(3), 572–578 (2000)
- Lake, L.W., Johns, R., Rossen, B., Pope, G.A.: *Fundamentals of Enhanced Oil Recovery*. Society of Petroleum Engineers Richardson, TX (2014)
- Lee, T., Bocquet, L., Coasne, B.: Activated desorption at heterogeneous interfaces and long-time kinetics of hydrocarbon recovery from nanoporous media. *Nat. Commun.* **7**, 11890 (2016)
- Li, Y., Orr, F.M., Benson, S.M.: Long-term redistribution of residual gas due to non-convective transport in the aqueous phase. *Transp. Porous Media* **141**(1), 231–253 (2022)
- Li, Y., Garing, C., Benson, S.M.: A continuum-scale representation of Ostwald ripening in heterogeneous porous media. *J. Fluid Mech.* 889, (2020)
- Lifshitz, I.M., Slyozov, V.V.: The kinetics of precipitation from supersaturated solid solutions. *J. Phys. Chem. Solids* **19**(1–2), 35–50 (1961)
- Lu, Z., Daino, M.M., Rath, C., Kandlikar, S.G.: Water management studies in PEM fuel cells, part III: dynamic breakthrough and intermittent drainage characteristics from GDLs with and without MPLs. *Int. J. Hydrogen Energy* **35**(9), 4222–4233 (2010)
- Mantzaris, N.V.: Liquid-phase synthesis of nanoparticles: particle size distribution dynamics and control. *Chem. Eng. Sci.* **60**(17), 4749–4770 (2005)
- Meinders, M.B., van Vliet, T.: The role of interfacial rheological properties on Ostwald ripening in emulsions. *Adv. Colloid Interface Sci.* **108–109**, 119–126 (2004)
- Nield, D.A., Bejan, A.: *Convection in Porous Media*. Springer, Heidelberg (2006)
- Saripalli, K.P., Serne, R.J., Meyer, P.D., McGrail, B.P.: Prediction of diffusion coefficients in porous media using tortuosity factors based on interfacial areas. *Ground Water* **40**(4), 346–352 (2002)
- Slezov, V.V., Schmelzer, J., Möller, J.: Ostwald ripening in porous materials. *J. Cryst. Growth* **132**(3–4), 419–426 (1993)
- Venzl, G.: Dynamics of first-order phase transitions: theory of coarsening (Ostwald ripening) for open systems. *Phys. Rev. A Gen. Phys.* **31**(5), 3431–3440 (1985)
- Voorhees, P.W.: The theory of Ostwald ripening. *J. Stat. Phys.* **38**(1), 231–252 (1985)
- Wagner, C.: Theorie der alterung von niederschlägen durch umlösen (Ostwald-reifung). *Zeitschrift Für Elektrochem. Berichte Der Bunsengesellschaft Für Phys. Chem.* **65**(7–8), 581–591 (1961)
- Wang, C., Mehmani, Y., Xu, K.: Capillary equilibrium of bubbles in porous media. *Proc. Natl. Acad. Sci.* **118**(17), e2024069118 (2021)
- Xu, K., Bonnecaze, R., Balhoff, M.: Egalitarianism among bubbles in porous media: an Ostwald ripening derived Anticoarsening phenomenon. *Phys. Rev. Lett.* **119**(26), 264502 (2017)
- Xu, K., Mehmani, Y., Shang, L., Xiong, Q.: Gravity-induced bubble ripening in porous media and its impact on capillary trapping stability. *Geophys. Res. Lett.* **46**(23), 13804–13813 (2019)
- Yec, C.C., Zeng, H.C.: Synthesis of complex nanomaterials via Ostwald ripening. *J. Mater. Chem. A* **2**(14), 4843–4851 (2014)

**Publisher's Note** Springer Nature remains neutral with regard to jurisdictional claims in published maps and institutional affiliations.